Multichannel Molecular Switch with a Surface-Confined Electroactive Radical Exhibiting Tunable Wetting Properties

ARTICLE *in* NANO LETTERS · SEPTEMBER 2011

Impact Factor: 13.59 · DOI: 10.1021/nl2025097 · Source: PubMed

4 AUTHORS:

Claudia C. D. Simao
Eurecat
27 PUBLICATIONS **184** CITATIONS
SEE PROFILE

Marta Mas-Torrent
Materials Science Institute of Barcelona
118 PUBLICATIONS **2,369** CITATIONS
SEE PROFILE

Jaume Veciana
Spanish National Research Council
981 PUBLICATIONS **12,291** CITATIONS
SEE PROFILE

Concepcio. Rovira
Spanish National Research Council
528 PUBLICATIONS **9,025** CITATIONS
SEE PROFILE

nature chemistry

ARTICLES

PUBLISHED ONLINE: 27 MARCH 2011 | DOI: 10.1038/NCHEM.1013

A robust molecular platform for non-volatile memory devices with optical and magnetic responses

Cláudia Simão[1,2], Marta Mas-Torrent[1,2], Núria Crivillers[1,2], Vega Lloveras[1], Juan Manuel Artés[3], Pau Gorostiza[3,4,5], Jaume Veciana[1,2]* and Concepció Rovira[1,2]*

Bistable molecules that behave as switches in solution have long been known. Systems that can be reversibly converted between two stable states that differ in their physical properties are particularly attractive in the development of memory devices when immobilized in substrates. Here, we report a highly robust surface-confined switch based on an electroactive, persistent organic radical immobilized on indium tin oxide substrates that can be electrochemically and reversibly converted to the anion form. This molecular bistable system behaves as an extremely robust redox switch in which an electrical input is transduced into optical as well as magnetic outputs under ambient conditions. The fact that this molecular surface switch, operating at very low voltages, can be patterned and addressed locally, and also has exceptionally high long-term stability and excellent reversibility and reproducibility, makes it a very promising platform for non-volatile memory devices.

Molecular surface engineering aims to design surfaces with specifically tailored properties (such as wettability and workfunction) by functionalization with appropriately chosen molecules[1,2]. A groundbreaking approach in this field is the preparation of stimuli-responsive surfaces[3], also known as smart surfaces, which can operate as switches or memory bits and have potential applications in (bio)sensors and (opto)electronic devices[4,5]. To achieve this potential, bistable systems are required that can be switched by an external trigger and produce a non-destructive readout. Although molecular switches in solution have been studied for many years[6], switches based on self-assembled monolayers (SAMs) located on surfaces, which are crucial for device implementation, are still rare, and only a few examples have been reported[7–10]. Of these, most are based on molecules that undergo photo- or electro-induced reactions associated with changes in their conformation[8–10], electroactivity[11], wettability[12], chemical sensing ability[13–16] or optical absorption[17–20]. Particularly outstanding is the work initiated by Di Bella[17] and expanded by van der Boom[19], which is based on redox switches of self-assembled metallic complexes coupled with changes in optical absorbance. These functionalized surfaces have recently been proven to comprise a versatile platform for the integration of binary logic gates[21–23]. Here, we report a highly robust surface-confined switch based on an organic polychlorotriphenylmethyl (PTM) radical. The patternability and local addressability of this electrochemical switch, combined with its unprecedented reproducibility and stability under ambient conditions, opens up the range of applications of such molecules in practical electronic devices. In addition, to our knowledge, this is the first example of a surface molecular switch in which an electrical input is transduced into both optical and magnetic outputs. The approach used is also suitable for extension to other stable organic electroactive molecules.

Results and discussion

Members of the family of PTM radicals are chemically and thermally persistent due to the fact that their open-shell centres are shielded by six bulky chlorine atoms[24]. In addition, they are bistable in terms of their electroactive character, as they can be easily and reversibly reduced to the carboanion form. Because this redox process occurs at very low potentials, these molecules are promising for applications in charge storage memory devices. The redox pair also demonstrates unequivocally different magnetic and optical properties: the PTM radical is a paramagnetic species with maximum absorbance centred at 385 nm and fluorescence emission at 688 nm, but the anion is diamagnetic, with a maximum absorbance at ~510 nm, and does not emit fluorescence. Previously, we have reported the fabrication and characterization of PTM radical SAMs on substrates such as silicon oxide, quartz and gold[25–27]. The current work focuses on investigating the electrochemically triggered switching properties of SAMs of radical **1** on indium tin oxide (ITO) (Fig. 1). This substrate is conducting and transparent, and therefore allows electrochemical triggering of the state of the switch while at the same time allowing the optical (absorbance and emission) and magnetic properties to be monitored.

Novel PTM radical derivative **1**, bearing a silane moiety, was synthesized to anchor directly on metal oxide surfaces. Synthesis was carried out by means of a condensation reaction with tetradecachloro-4-(hydroxymethyl)triphenylmethyl radical (**2**)[28] and triethoxy(3-isocyanatopropyl)silane (ICTES), resulting in radical **1** in high yield (80%) (Fig. 2). SAMs of **1** on glass coated with ITO substrates were fabricated by immersing freshly cleaned substrates in a 1 mM solution of **1** in toluene for 24 h. Subsequently, the functionalized substrates were rinsed thoroughly with toluene and dried under a nitrogen stream.

[1]Institut de Ciència de Materials de Barcelona (CSIC), Campus de la UAB, 08193 Bellaterra, Spain, [2]Networking Research Center on Bioengineering, Biomaterials and Nanomedicine (CIBER-BBN). Campus de la UAB, 08193 Bellaterra, Spain, [3]Institute for Bioengineering of Catalonia (IBEC), Baldiri Reixac 15-21 08028 Barcelona, Spain, [4]Institució Catalana de Recerca i Estudis Avançats (ICREA), [5]Networking Research Center on Bioengineering, Biomaterials and Nanomedicine (CIBER-BBN), Universitat de Barcelona, C/ Martí i Franquès, 1 Barcelona, 08028 Barcelona, Spain. *e-mail: cun@icmab.es; vecianaj@icmab.es

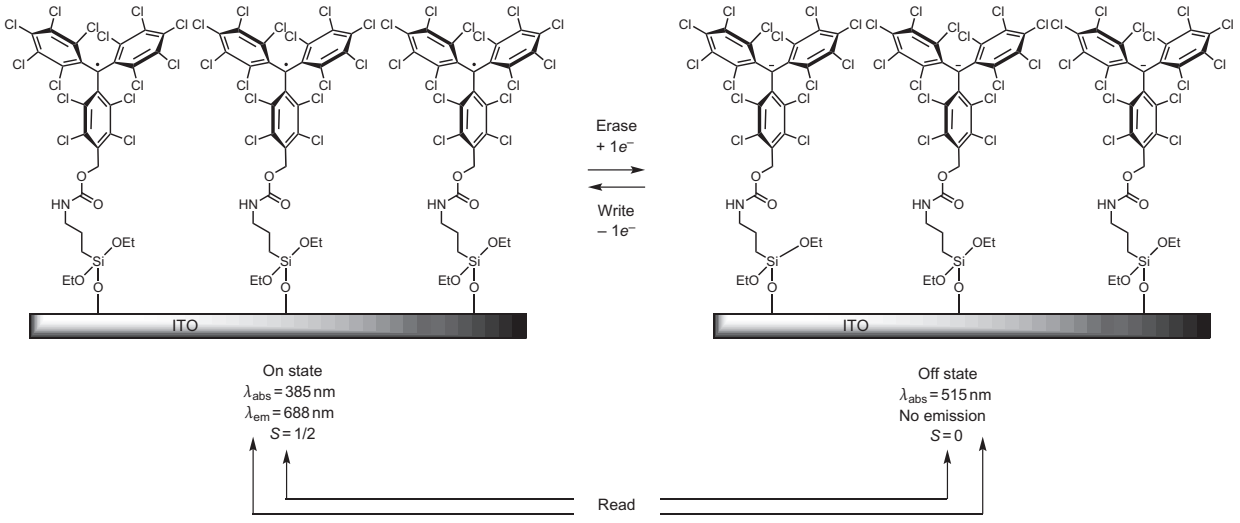

Figure 1 | Representation of the electrochemical bistability of a SAM of PTM radical 1. The PTM molecule has two redox states, the radical (left) and anion (right) forms, which can be electrochemically interconverted. Each state exhibits different magnetic and optical properties: radical SAM **1** exhibits spin $S = 1/2$, an absorbance band at 385 nm and fluorescence with emission at 688 nm, and anion SAM $\mathbf{1}^-$ is a diamagnetic species with $S = 0$, a maximum absorbance band at 515 nm, and is not fluorescent.

Characterization of the surfaces by X-ray photoelectron spectroscopy (XPS) following functionalization revealed the disappearance of the peaks corresponding to tin and indium, accompanied by the emergence of new peaks related to the presence of the organic monolayer, namely silicon and chlorine, and an increase in the peaks associated with carbon, oxygen and nitrogen (Supplementary Fig. S1). Time-of-flight secondary ion mass spectrometry (ToF–SIMS) showed the molecular peak at 667.6 m/z, with the typical isotopic chlorine distribution of PTM radical molecules, attributed to the ionized species PTM–CH_2^+ with loss of two chlorine atoms (Supplementary Fig. S2). UV-vis and electron paramagnetic resonance (EPR) spectra of the SAM of **1** were also recorded in air to confirm the chemical nature of the SAM. The UV-vis spectrum showed an absorption band centred at 385 nm, assigned to the triphenylmethyl radical unit[25–27]. The EPR spectrum further confirmed that the radical character was preserved, with a signal at a g-value of 2.0027 and a linewidth of 4.7 G typical of a PTM radical in the solid state (Supplementary Fig. S3)[25,29].

The electrochemical characteristics of the PTM radical SAMs were investigated by cyclic voltammetry (CV). Experiments were carried out in a 0.02 M solution of tetrabutylammonium hexafluorophosphate in acetonitrile, using the functionalized substrate as the working electrode (versus $Ag_{(s)}$). Figure 3a presents a cyclic voltammogram showing one reversible redox wave with an oxidation peak at +53 mV and a reduction peak at −32 mV at a scan rate 100 mV s^{-1}. It was also observed that the current linearly increased with scan rate, which is characteristic of surface-confined

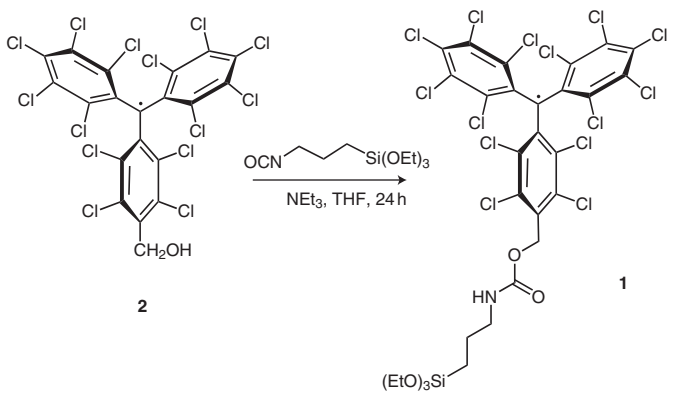

Figure 2 | Synthesis of PTM radical 1. A condensation reaction between the triethoxy(3-isocyanatopropyl)silane and a PTM radical core bearing an alcohol moiety resulted in the desired radical **1** in high yield.

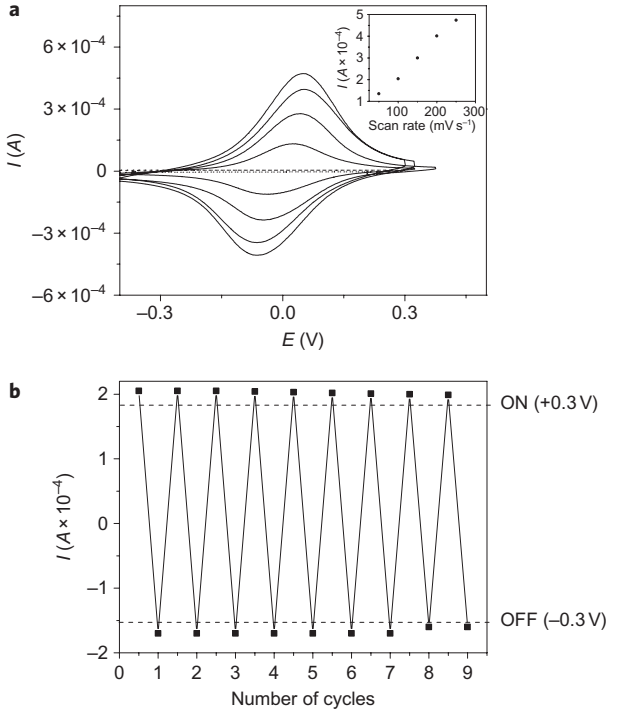

Figure 3 | Electrochemical characteristics of SAMs of 1. a, Cyclic voltammogram at different scan rates (50, 100, 150, 200 mV s^{-1}) of a SAM of **1** on an ITO substrate (versus silver wire) in an electrolyte solution of 0.02 M tetrabutylammonium hexafluorophosphate in acetonitrile. Inset: plot of anodic current versus scan rate. **b**, Anodic and cathodic current intensity registered during nine consecutive CV cycles at 100 mV s^{-1}, showing the excellent recovery of current values from the ON (radical) and OFF (anion) states and the high reversibility of the process.

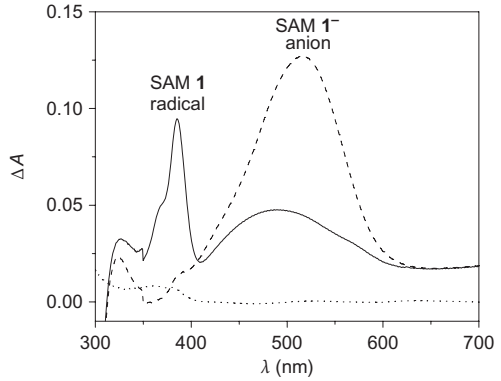

Figure 4 | Optical absorption of the two states of the SAM of 1. UV-vis absorption spectra of ITO functionalized with PTM radical **1** (solid line) and after *in situ* electrochemical reduction on applying −0.3 V to the substrate for 30 s (dashed line). Electrochemical reduction was performed using a platinum wire as counterelectrode, a silver wire as reference electrode and, as electrolyte, a 0.02 M solution of tetrabutylammonium hexafluorophosphate in acetonitrile. The dotted line corresponds to the absorbance of the bare ITO substrate.

electroactive species (Fig. 3a, inset). The surface coverage (Γ) of the SAM was estimated from anodic charge integration at 100 mV s^{-1}, giving a high coverage value of 4×10^{-10} mol cm^{-2}. The stability of the two redox states was confirmed by performing many consecutive voltage cycles, which resulted in completely identical redox waves without any sign of loss of current intensity (Fig. 3b). This was an encouraging result indicating the excellent potential of these SAMs to function as reversible and extremely stable switches.

To achieve read/write memory devices it is imperative for there to be a secondary physical signal in order to be able to read the state of the switch non-destructively. We first used the optical absorption and emission responses and subsequently the magnetic response. Figure 4 presents the evolution of the UV-vis spectra of the SAM of radical **1** when a voltage of −0.3 V is applied to the functionalized ITO substrate and the SAM of anion $\mathbf{1}^-$ is formed. Such spectroelectrochemical experiments clearly show that the two redox states of the SAM can be easily identified from the UV-vis spectra, as both forms exhibit distinct intense absorption bands (385 nm for the PTM radical and 515 nm for the PTM anion), thereby demonstrating that optical readout of the charge storage is viable. It should be noted, however, that the SAM of the radical shows a broad absorption band at ∼480 nm that does not originate from the PTM radical but instead from the functionalization of the ITO with a silane moiety (Supplementary Fig. S4). Electrochemical switching was also followed by fluorescence microscopy analysis (Supplementary Fig. S5 and Video S1).

An important factor that should be considered in developing molecular devices is the time response of the switch, which we studied here by electrochemical means and also by following the UV-vis response over time. From the CV characteristics it was possible to calculate the heterogeneous electron transfer constant rates k_{ET}, according to Laviron's approach to Butler–Volmer theory[30]. This theory is based on the loss of reversibility of the redox reaction on the surface on applying higher scan rates due to kinetic effects; this is illustrated by an increase in voltage difference between the oxidation and reduction peaks (ΔE_p). The k_{ET} values found for both reduction and oxidation processes were 19 s^{-1}. This value is of the same order of magnitude as those reported for SAMs of other electroactive species on ITO, such as benzo(c)cinnoline at pH 8.70 (38.9 s^{-1})[30], horse cytochrome *c* (10 s^{-1})[31] and a ferrocene-based monolayer (9 s^{-1})[32].

The evolution of the radical and anion absorption bands was then plotted during their interconversion while applying 30 s voltages pulses of +0.3 and −0.3 V to the ITO-functionalized substrate. As shown in Fig. 5, in both cases there is an initial fast optical response, with immediately high on/off ratios. For the absorption band at 385 nm, we found that in ∼1 s the absorbance reached 95% of its maximum value (or in 87 ms, 20%). However, achieving a steady absorbance value takes ∼10 additional seconds for radical formation and ∼15 s more for the anion. These distinct characteristic profiles introduce individual imprints in the optical output for each redox species, which can be monitored because they are related to the kinetics of the system. Both redox reactions seem to be subject to two constant rates, a fast one that dominates the process and depends on the magnitude of the applied voltage (Supplementary Fig. S6), and a much slower one that is driven by counterion diffusion. Importantly, once either of the two redox states of the SAM is formed, the optical response does not deteriorate for several hours, demonstrating the long-term stability of the two states of the switch (Supplementary Fig. S7).

The reversibility of the switch was investigated by monitoring the absorbance of the SAM while performing write–erase cycles, switching the SAM of **1** between the radical (ON state) and anion (OFF state) forms. In a process similar to that reported previously for a ruthenium-based monolayer[19], we observed that the conversion to the OFF state takes from two to four cycles before achieving a stable absorbance value. In the present system, this effect can be attributed to SAM reorganization occurring during the early cycles due to diffusion of counterions through the monolayer, and it is reminiscent of the common training period found in many sensor devices. Figure 6a,b shows the optical response of the switch on application of alternating 30 s voltage pulses of +0.3 V (write) and −0.3 V (erase) while monitoring the optical absorbance (read) at $\lambda_{abs} = 385$ nm (SAM radical **1**) and 515 nm (SAM anion $\mathbf{1}^-$). The two absorption bands change simultaneously in opposite directions, following the profile of the applied voltages in a completely reversible way and recovering the absorption intensity completely after each cycle. This behaviour clearly reveals the excellent performance of the switch. In Fig. 6a, 65 consecutive cycles are plotted, but, in fact, hundreds of switching cycles were applied on different days and the SAM showed no hints of degradation, demonstrating the exceptionally high robustness of the system (Supplementary Fig. S8). Even after three months at ambient conditions, the switch continued to operate reliably (Supplementary Fig. S9).

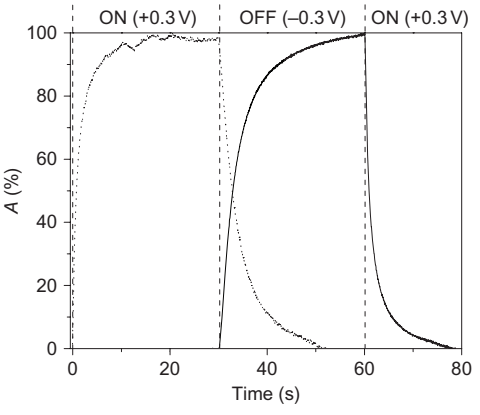

Figure 5 | Time response of the switch. UV-vis absorbance against time for a SAM of **1** on application of +0.3 V (ON state) and −0.3 V (OFF state) to the ITO-functionalized substrate, in an *in situ* electrochemical experiment using a silver wire as reference electrode and an electrolyte solution of 0.02 M tetrabutylammonium hexafluorophosphate in acetonitrile. The dashed line corresponds to the absorbance at 385 nm, the solid line to absorbance at 515 nm.

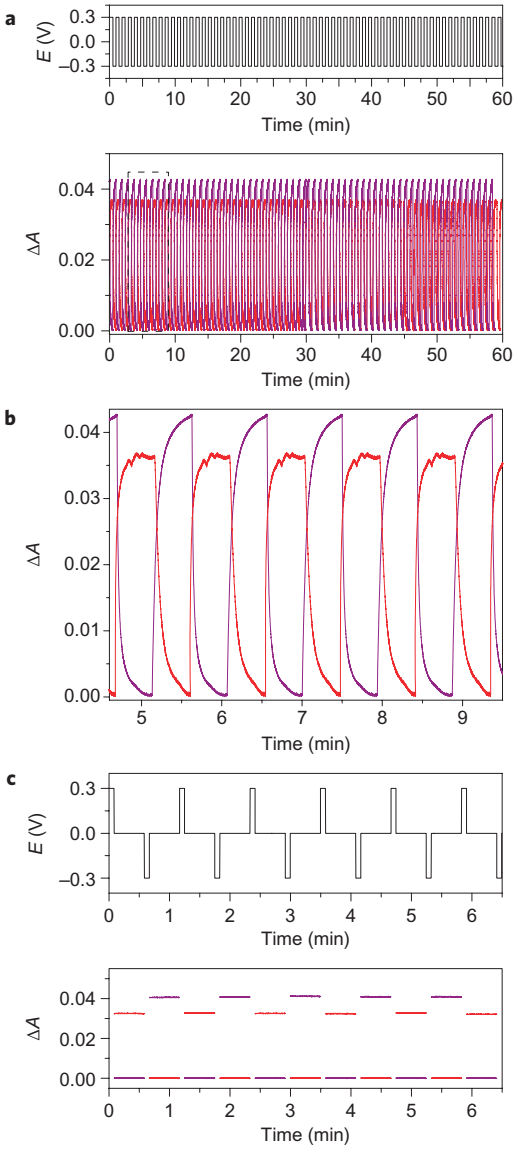

Figure 6 | Measure of the optical response of the switch. a, Bottom: optical response versus time during 65 consecutive write–erase cycles (+0.3 V/−0.3 V versus Ag(s)) applied to a SAM of radical **1** monitored at 385 nm (black line) and 515 nm (grey line). The electrochemical experiment was performed *in situ* using a UV-vis cuvette, a silver wire as reference electrode and an electrolyte solution of 0.02 M tetrabutylammonium hexafluorophosphate in acetonitrile. Top: voltage profile applied to a SAM of **1**. **b**, Enlarged view of the area marked in **a**. **c**, Sequence of write–read–erase–read pulses (+0.3 V/0V/−0.3 V/0 V versus Ag(s)) applied to a SAM of **1** (top), and the optical response (bottom) monitored at 385 nm (black line) and 515 nm (grey line) during the reading processes.

To further demonstrate the potential of this system to build non-volatile memory devices, the switch response to a sequence of write–read–erase–read pulses was investigated. Short 5 s write (+0.3 V) and erase (−0.3 V) pulses were applied, while reading the state of the switch was performed for 30 s at 0 V. As can be seen in Fig. 6c, both states of the switch were completely stable and reproducible.

As previously mentioned, the magnetic output can also be used to read the state of the switch, because the radical species is paramagnetic ($S = 1/2$) and the anion is diamagnetic ($S = 0$). To demonstrate this, the electrochemical switch was monitored by EPR. The electrochemistry was carried out in a conventional electrochemical cell outside the EPR cavity, and voltage pulses of +0.3 V and −0.3 V were applied for 2 min. In each reduction and oxidation step, the functionalized surface was extracted from the electrolyte solution and its EPR spectra measured immediately in air. Figure 7 shows the EPR response when ten consecutive electrochemical cycles were applied. It was observed that the EPR signal, corresponding to the PTM radical immobilized on the surface[25–27] (ΔH_{pp}(SAM of **1**) = 4.7 G; Supplementary Fig. S3), practically disappeared on reduction to the anionic form. Only a residual signal at $g = 2.0013$ could be detected that resulted from the ITO substrate. As can be seen, the process is fully reproducible, and there is full signal recovery after each cycle, confirming again the excellent reversibility of the surface switching process and also that the magnetic characteristics can also provide a suitable readout tool with which to determine the state of the switch.

In view of the above, SAMs based on **1** offer great potential for use in binary logic gates[21–23,33,34]. The applied voltage can be considered as the input; that is, when +0.3 V is applied the SAM is in the radical form (input = 1), and when −0.3 V is applied the SAM is in the anionic state (input = 0). In fact, four different outputs can be defined: the absorption band at $\lambda_{abs} = 385$ nm (output 1), the absorption band at $\lambda_{abs} = 515$ nm (output 2), the fluorescence emission at $\lambda_{em} = 688$ nm (output 3) and the EPR signal (output 4). As there are four different outputs for the same input, it is possible to define four different logic gates or, alternatively, to combine the four outputs in one system. Table 1 presents the truth table of this system.

The functional PTM molecules were locally confined on the ITO substrate using a microcontact printing technique (Supplementary Fig. S10). The switching properties of these patterned surfaces have also been demonstrated (Supplementary Fig. S11). Importantly, by using a microelectrode, one can locally address the redox switch as shown in Supplementary Fig. S12, in which two dots from a PTM-patterned surface have been switched off and on consecutively, and visualized with a fluorescence microscope. The fabrication of such an array of memory elements represents a significant step towards the exploitation of these systems for practical devices such as electronic tags, sensors or biomolecule dispensers.

In summary, a SAM of an organic bistable radical on ITO has been investigated for the first time as a surface molecular switch. Owing to its electroactive character, the SAM was reversibly

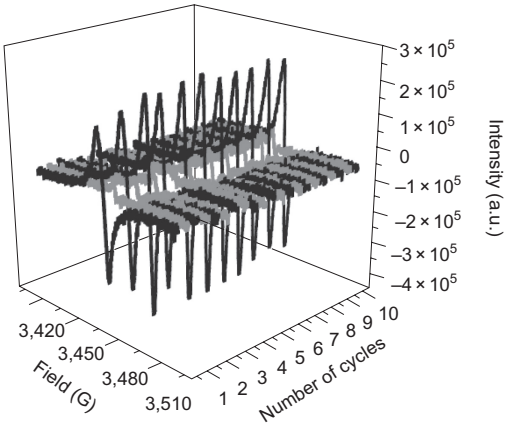

Figure 7 | Measure of the magnetic response of the switch. EPR signal of a SAM of radical **1** on ITO, in air, on application of ten *ex situ* electrochemical ON/OFF switching cycles of +0.3 V (radical **1**) and −0.3 V (anion **1**$^-$) using a silver wire as reference electrode, platinum wire as counterelectrode and an electrolyte solution of 0.02 M tetrabutylammonium hexafluorophosphate in acetonitrile. Black corresponds to the ON state (radical **1**) and grey to the OFF state (anion **1**$^-$).

Table 1 | Truth table for the binary logic functions of the SAM of 1.

Input (V = +0.3 V; −0.3 V)	Output 1 λ_{abs} = 385 nm	Output 2 λ_{abs} = 515 nm	Output 3 λ_{em} = 688 nm	Output 4 EPR signal
1 (radical)	1	0	1	1
0 (anion)	0	1	0	0

interconverted between two redox states (the radical and anion forms). In addition, we have shown that the inherent magnetic moment that organic radicals exhibit can be exploited. Indeed, the magnetic response can be used as a readout mechanism, as well as the optical response. The extremely high robustness, long-term stability, reversibility and reproducibility of the switch, the fact that it can be patterned and locally addressed, and also that it operates at very low voltages makes this system very promising in the development of non-volatile memory devices based on immobilized molecules, which is of great interest in the field of molecular electronics.

Methods

The reagents and solvents used for synthesis were of high purity grade (Sigma-Aldrich and SDS SA). The solvents used in the surface chemistry experiments were of high purity grade for HPLC from ROMIL-SpS (Super Purity Solvent). The ITO substrates were purchased from Delta Technologies, as double-face-coated ITO over unpolished float glass with a resistance of 15–25 Ω. The dimensions of the substrates were 7 × 50 × 0.5 mm^3 for electrochemical and UV-vis experiments and 3 × 150 × 0.5 mm^3 for EPR measurements.

The electrochemical experiments were performed with a potentiostat-galvanostast 263a (EG&G Princeton Applied Research) using a platinum wire as counterelectrode, a silver wire as reference electrode and as electrolyte a 0.02 M solution of tetrabutylammonium hexafluorophosphate (TBAHFP) in acetonitrile. For the EPR electrochemical experiments a standard 25 ml cylindrical cell was used, and for the UV-vis electrochemical experiments a homemade setup, adapting the standard 1 cm optical pathway quartz SUPRASIL cuvette from Hellma GmbH as an electrochemical cell. After all electrochemical experiments, the functionalized ITO electrode was removed and the optical absorption of the electrolyte solution was examined to ensure that no material had been desorbed from the substrate during the experiments. XPS experiments were performed with a PHI 5500 Multitechnique System (Physical Electronics) with a monochromatic X-ray source (AlKα line of 1,486.6 eV energy and 350 W) placed perpendicular to the analyser axis and calibrated using the $3d_{5/2}$ line of silver with a full-width at half-maximum (FWHM) of 0.8 eV. The analysed area was a circle with a diameter of 0.8 mm. The resolution chosen for the spectra was 187.5 eV of pass energy and 0.8 eV per step for the general spectra and 23.5 eV of pass energy and 0.1 eV per step for the spectra of the different elements. All measurements were made in an ultrahigh-vacuum chamber at a pressure between 5×10^{-9} and 2×10^{-8} torr. The ToF–SIMS measures were recorded with a ToF–SIMS IV mass spectrometer (Ion-Tof GmbH) equipped with a bismuth cluster (Bi3) ion source. The primary ions hit the surface of the sample with a kinetic energy of 25 keV and an incidence angle of 45°. The primary ion current, measured with a Faraday cup on the sample holder, was 0.2 pA for Bi^{3+} at 10 kHz. The primary ion dose was between 4.7×10^{11} ions cm^{-2} and 1,012 ions cm^{-2}. The secondary ions were extracted with an energy of 2 keV and were post-accelerated to 10 keV just before hitting the detector surface (single channel plate followed by a scintillator and a photomultiplier). A low-energy electron flood gun was activated to neutralize the surface during analysis. The effective ion flight path was 2 m in length (using a reflectron), and the mass resolution was greater than 8,000 FWHM at m/z = 35 and 10,000 (FWHM) at m/z = 795.7. The scan area was 125 × 125 μm^2 (256 × 256 pixels).

Optical absorption measurements were carried out using a Cary 5000 UV-vis-NIR spectrophotometer in double-beam mode, using as reference sample a blank ITO inside the electrolyte solution used in the electrochemical experiments. Fluorescence microscopy was recorded with a Nikon E1000 microscope, using mercury lamp excitation with a UV filter (λ_{exc} = 340–370 nm), and emission was recorded using a DAPI filter.

EPR measurements were performed at room temperature using a Bruker ELEXYS E500 X-band spectrometer in a rectangular TE102 cavity. Precautions to avoid undesirable spectral distortions and line broadenings, such as those arising from microwave power saturation and magnetic field overmodulation, were also taken into account to improve sensitivity.

Synthesis of tetradecachloro-4-(3(1-triethoxysilylpropyl)formamidyl)oxymethyl triphenylmethyl radical (1). Under argon and light exclusion, ICTES (64 μl; 0.25 mmol) and triethylamine (35.5 μl; 0.25 mmol) were consecutively added to a solution of hydroxymethyl radical **2** (150 mg; 0.16 mmol) in 3 ml of dry tetrahydrofuran (THF). The mixture was then stirred for 24 h. The solvent was then evaporated, producing a red oil. Recrystallization from pentane at 5 °C overnight returned a red solid that was characterized as the desired product (175 mg; 80%). IR (ATR) (ν/cm^{-1}): 3,298 (w), 2,974 (m), 2,927 (m), 2,881 (m), 1,727 (m), 1,698 (s), 1,539 (s), 1,427 (m), 1,363 (m), 1,338 (m), 1,297 (m), 1,245 (s), 1,076 (w), 1,003 (m), 954 (s), 856 (w), 808 (s), 768 (m), 689 (w), 650 (m), 515(m). UV-Vis (CH_2Cl_2) (nm): 220, 289, 369 (sh), 386, 509, 565 (ε, 81,000, 6,600, 17,800, 35,000, 1,100, 1,020); EPR (CH_2Cl_2): 1 line; g = 2.0027; ΔH_{pp} 1.34 G (solution); 5,7 (solid); cyclic voltammetry (0.1 M TBAHFP in CH_2Cl_2 versus Ag/AgCl): $E_{1/2}$ = 0.013 V. Elemental analysis: calc. For $C_{30}H_{24}Cl_{14}NO_5Si$, C (35.89%), H (2.51%), N (1.40%); expt.: C (36.00%), H (2.54%), N (1.48%); LDI-TOF m/z (%): 956.1 ([M^+], 100), calc.: 952.95.

Preparation of the self-assembled monolayers (SAMs). The ITO substrates were first degreased in ultrasonic baths using a solvent series with increased polarity: dichloromethane, acetone and then ethanol for 15 min each. The substrates were rinsed with pure ethanol and dried under a nitrogen stream. The substrates were then treated in an oxidizing bath of NH_4OH:H_2O_2:H_2O (1:1:5) at 80 °C for 30 min and washed thoroughly with millipore distilled water, rinsed with ethanol and then dried under a nitrogen stream. The freshly cleaned ITO substrates were immersed in a 1 mM solution of radical **1** in freshly distilled toluene, in a vessel under argon atmosphere. After 24 h, the substrates were washed thoroughly with toluene and dried under a smooth nitrogen stream giving radical **1** functionalized ITO substrates.

Patterning of SAMs. Poly(dimethylsiloxane) (PDMS) stamps were fabricated by pouring a 10:1 (v/v) mixture of Sylgard 184 elastomer and curing agent over a patterned silicon master. The stamps were inked in a 0.1 M solution of **1** in THF:CH_3CN (3:7) by immersing them for 3 min. The stamp was removed from solution, dried under a nitrogen stream and brought into contact with the ITO substrate for 5 min, then dried smoothly under nitrogen. The pattern was visualized by fluorescence microscopy with excitation from a mercury lamp with a UV filter (λ_{exc} = 340–370 nm), and the red fluorescence of grafted radical **1** was observed with a DAPI filter.

Fluorescence switching experiments. PTM SAMS on ITO in an electrolyte chamber were imaged with an inverted fluorescence microscope (Olympus IX71, ×10 objective, excitation of 380 nm, emission at 500 nm) coupled to a Hamamatsu imagEM charge-coupled device (CCD) camera. Fluid chamber and microelectrode fabrication for the local application of potentials is detailed in the Supplementary Information.

Received 27 July 2010; accepted 17 February 2011; published online 27 March 2011

References

1. Wöll, C. Interfacial systems chemistry: towards the remote control of surface properties. *Angew. Chem. Int. Ed.* **48,** 8406–8408 (2009).
2. Heimel, G., Romaner L., Zojer, E. & Brédas, J.-L. The interface energetics of self-assembled monolayers on metals. *Acc. Chem. Res.* **41,** 721–729 (2008).
3. Mendes, P. M. Stimuli-responsive surfaces for bio-applications. *Chem. Soc. Rev.* **37,** 2512–2529 (2008).
4. Kronemeijer, A. J. *et al.* Reversible conductance switching in molecular devices. *Adv. Mater.* **20,** 1467–1473 (2008).
5. Mativetsky, J. M. *et al.* Azobenzenes as light-controlled molecular electronic switches in nanoscale metal–molecule–metal junctions. *J. Am. Chem. Soc.* **130,** 9192–9193 (2008).
6. Photochromism: Memories and switches. *Chem. Rev.* **100**(special issue), 6–1890 (2000).
7. Liu, Z., Yasseri, A. A., Lindsey, J. S. & Bocian, D. F. Molecular memories that survive silicon device processing and real-world operation. *Science* **302,** 1543–1545 (2003).
8. Katsonis, N. *et al.* Reversible conductance switching of single diarylethenes on a gold surface. *Adv. Mater.* **18,** 1397–1400 (2006).
9. Namiki, K., Sakamoto, A., Murata, M., Kume, S. & Nishihara, H. Reversible photochromism of a ferrocenylazobenzene monolayer controllable by a single green light source. *Chem. Commun.* 4650–4652 (2007).
10. Sortino, S., Petralia, S., Conoci, S. & Di Bella S. Monitoring photoswitching of azobenzene-based self-assembled monolayers on ultrathin platinum films by UV/vis spectroscopy in the transmission mode. *J. Mater. Chem.* **14,** 811–813 (2004).
11. Areephong, J., Browne, W. R., Katsonis, N. & Feringa, B. L. Photo- and electro-chromism of diarylethene modified ITO electrodes—towards molecular based read–write–erase information storage. *Chem. Commun.* 3930–3932 (2006).
12. Lahann, J. *et al.* A reversibly switching surface. *Science* **299,** 371–374 (2003).
13. de Ruiter, G. Gupta, T. & van der Boom, M. E. Selective optical recognition and quantification of parts per million levels of Cr^{6+} in aqueous and organic media by immobilized polypyridyl complexes on glass. *J. Am. Chem. Soc.* **130,** 2744–2745 (2008).

14. Gupta, T. & van der Boom, M. E. Monolayer-based selective optical recognition and quantification of $FeCl_3$ via electron transfer. *J. Am. Chem. Soc.* **129,** 12296–12303 (2007).
15. Gupta, T. & van der Boom, M. E. Optical sensing of parts per million levels of water in organic solvents using redox-active osmium chromophore-based monolayers. *J. Am. Chem. Soc.* **128,** 8400–8401 (2006).
16. Cook, M. J., Nygard, A.-M., Wang, Z. & Russell, D. A. An evanescent field driven mono-molecular layer photoswitch: coordination and release of metallated macrocycles. *Chem. Commun.* 1056–1057 (2002).
17. Sortino, S., Petralia, S., Conoci, S. & Di Bella, S. Novel self-assembled monolayers of dipolar ruthenium(III/II) pentaammine(4,4′-bipyridinium) complexes on ultrathin platinum films as redox molecular switches. *J. Am. Chem. Soc.* **125,** 1122–1123 (2003).
18. Sortino, S. *et al.* Electrochemical switching of chromogenic monolayers self-assembled on transparent platinum electrodes. *Adv. Mater* **17,** 1390–1393 (2005).
19. Shukla, A. D., Das, A. & van der Boom, M. E. Electrochemical addressing of the optical properties of a monolayer on a transparent conducting substrate. *Angew. Chem. Int. Ed.* **44,** 3237–3240 (2005).
20. Gupta, T. *et al.* Covalent assembled osmium-chromophore-based monolayers: chemically induced modulation of optical properties in the visible region. *Chem. Mater.* **18,** 1379–1382 (2006).
21. Gupta, T. & van der Boom, M. E. Chemical communication between metal-complex-based monolayers. *Angew. Chem. Int. Ed.* **47,** 2260–2262 (2008).
22. Gupta, T. & van der Boom, M. E. Redox-active monolayers as a versatile platform for integrating boolean logic gates. *Angew. Chem. Int. Ed.* **47,** 5322–5326 (2008).
23. de Silva, A. P. Molecular computing: a layer of logic. *Nature* **454,** 417–418 (2008).
24. Ballester, M., Riera, J., Castañer, J., Badia, C. & Monso, J. M.. Inert carbon free radicals. I. Perchlorodiphenylmethyl and perchlorotriphenylmethyl radical series. *J. Am. Chem. Soc.* **93,** 2215–2225 (1971).
25. Crivillers, N. *et al.* Self-assembled monolayers of a multifunctional organic radical. *Angew. Chem. Int. Ed.* **46,** 2215–2219 (2007).
26. Crivillers, N., Mas-Torrent, M., Vidal-Gancedo, J., Veciana, J. & Rovira, C. Self-assembled monolayers of electroactive polychlorotriphenylmethyl radicals on Au(111). *J. Am. Chem. Soc.* **130,** 5499–5506 (2008).
27. Crivillers, N. *et al.* Dramatic influence of the electronic structure on the conductivity through open- and closed-shell molecules. *Adv. Mater.* **21,** 1177–1181 (2009).
28. Ballester, M. *et al.* Inert carbon free radicals. 7. 'The (kinetic) reverse effect' and relevant synthesis of new monofunctionalized triphenylmethyl radicals and their nonradical counterparts. *J. Org. Chem.* **47,** 2472–2480 (1986).
29. Armet, O. *et al.* Inert carbon free radicals. 8. Polychlorotriphenylmethyl radicals. Synthesis, structure, and spin-density distribution. *J. Phys. Chem.* **91,** 5608–5616 (1987).
30. Laviron, E. General expression of the linear potential sweep voltammogram in the case of diffusionless electrochemical system. *J. Electroanal. Chem.* **101,** 19–28 (1979).
31. El Kasmi, A. *et al.* Adsorptive immobilization of cytochrome *c* on indium/tin oxide (ITO): electrochemical evidence for electron transfer-induced conformational changes. *Electrochem. Commun.* **4,** 177–181 (2002).
32. Li, J. *et al.* Characterization of transparent conducting oxide surfaces using self-assembled electroactive monolayers. *Langmuir* **24,** 5755–5765 (2008).
33. de Silva, A. P. & Uchiyama, S. Molecular logic and computing. *Nature Nanotech.* **2,** 399–410 (2007).
34. de Silva, A. P., James, M. R., McKinney, B. O. F., Pears, D. A. & Weir, S. M. Molecular computational elements encode large populations of small objects. *Nature Mater.* **5,** 787–790 (2006).

Acknowledgements

The research leading to these results received funding from the European Community's Seventh Framework Programme (FP7/2007-2013; grant 212311 (ONE-P project) and 210355 (OpticalBullet-ERC-StG project)), the Marie Curie Est FuMASSEC, the DGI (Spain) (grants EMOCIONa (CTQ2006-06333), POMAs (CTQ2010-19501) and Opticalswitch (CTQ2008-06160)), the Networking Research Center on Bioengineering, Biomaterials and Nanomedicine (CIBER-BBN), the Generalitat de Catalunya (grants 2009SGR00516 and 2009SGR00277) and the Human Frontier Science Program (HFSP, grant CDA0022/2006). The authors also thank Dr Vidal-Gancedo for his assessment of the EPR measurements, Dr S.T. Bromley for his advice and M. Izquierdo-Serra for help in the preparation of microelectrodes.

Author contributions

M.M-T., J.V. and C.R. conceived and designed the experiments. C.S. performed the experiments. N.C. contributed to SAM functionalization. V.L. contributed to EPR experiments. J.M.A. and P.G. contributed to fluorescence microscopy and local switching experiments. C.S. and M.M-T. co-wrote the paper with input from J.V. and C.R.

Additional information

The authors declare no competing financial interests. Supplementary information accompanies this paper at www.nature.com/naturechemistry. Reprints and permission information is available online at http://npg.nature.com/reprintsandpermissions/. Correspondence and requests for materials should be addressed to J.V. and C.R.

nature chemistry

SUPPLEMENTARY INFORMATION

DOI: 10.1038/NCHEM.1013

A Robust Molecular Platform for Nonvolatile Memory Devices with Optical and Magnetic Responses**

Cláudia Simão,[a,b] Marta Mas-Torrent,[a,b] Núria Crivillers,[a,b] Vega Lloveras,[a] Juan Manuel Artés,[c] Pau Gorostiza,[c,d,e] Jaume Veciana,[a,b]* Concepció Rovira[a,b]*

[a] *Institut de Ciència de Materials de Barcelona (CSIC), Campus de la UAB, 08193 Bellaterra, Spain*

[b] *Networking Research Center on Bioengineering, Biomaterials and Nanomedicine (CIBER-BBN). Campus de la UAB, 08193 Bellaterra, Spain*

[c] *Institute for Bioengineering of Catalonia (IBEC), Baldiri Reixac 15-21 08028 Barcelona, Spain*

[d] *Institució Catalana de Recerca i Estudis Avançats (ICREA).*

[e] *Networking Research Center on Bioengineering, Biomaterials and Nanomedicine (CIBER-BBN).Universidad de Barcelona. C/ Martí i Franqués, 1. Barcelona. 08028 Barcelona, Spain.*

1- Further characterization of SAM of **1** on ITO surfaces: XPS spectra, TOF-SIMS, EPR spectra

2- Further characterization of the switching process of SAM of **1** on ITO

3- Patterned surface of SAM of **1** on ITO, switching experiemtns and addressability of the switching process.

4- Supplementary Methods.

DOI: 10.1038/NCHEM.1013

CHARACTERISATIONS OF SAMs OF 1 ON ITO SURFACES

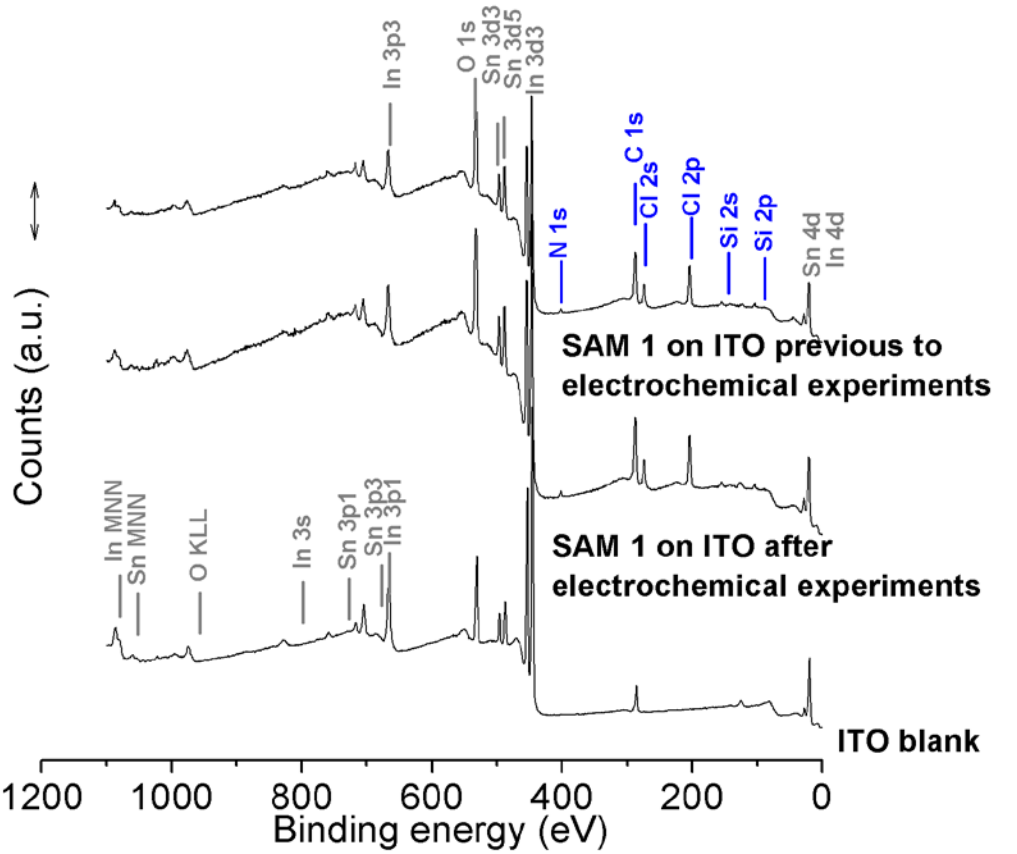

Figure S1. XPS spectra of a blank ITO surface (bottom) and of the SAM of **1** on ITO as prepared and after electrochemical switching (ECS) experiments.

Table S1. Ratios between peaks corresponding to PTM 1 and to ITO from XPS of Figure S1

	Cl2p/In3p3	Cl2p/Sn4d	C1s/In3p3	C1s/Sn4d
SAM 1 before ECS	0.589	0.791	0,683	0,918
SAM 1 after ECS	0.574	0.924	0,601	0,967

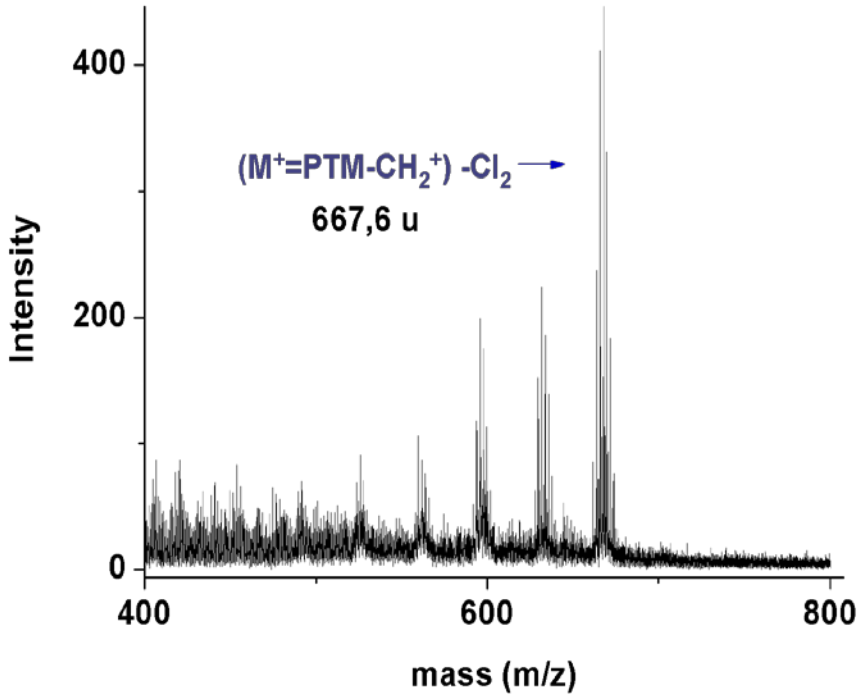

Figure S2. ToF-SIMS spectra of the SAM of **1** as prepared.

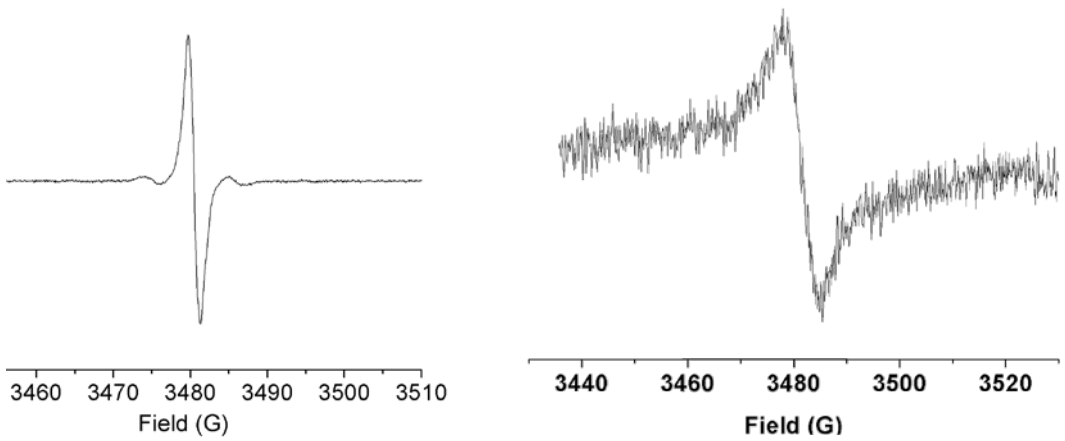

Figure S3. *Left,* isotropic EPR spectrum of **1** in solution of CH_2Cl_2 (ΔH_{pp} = 1.34 G). *Right*, EPR spectrum of the SAM of **1** on ITO in air (ΔH_{pp} = 4.7 G).

DOI: 10.1038/NCHEM.1013

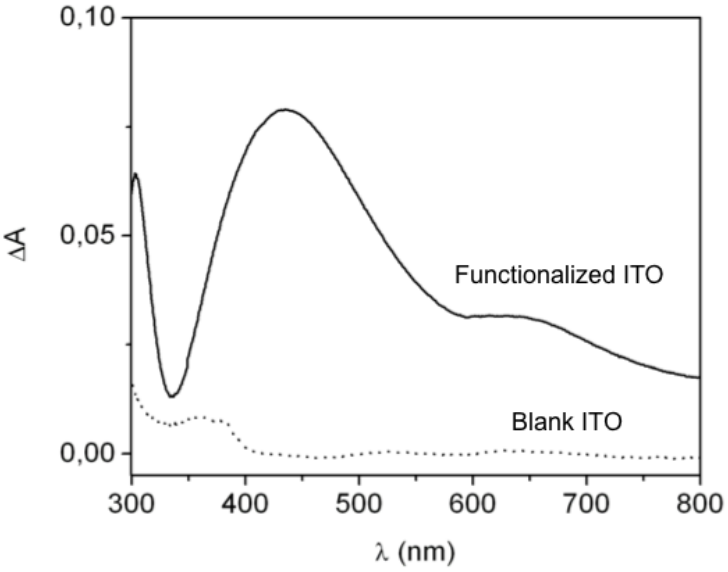

Figure S4. Blank UV-Vis absorbance spectra carried out to study the optical response of the SAM of **1** on ITO. Dotted line corresponds to the absorbance of a bare ITO substrate, whereas the continuous line corresponds to the absorbance of an ITO surface functionalized with octadecyltrichlorosilane (OTS).

CHARACTERISATION OF THE SWITCHING PROCESS OF SAMs OF 1 ON ITO

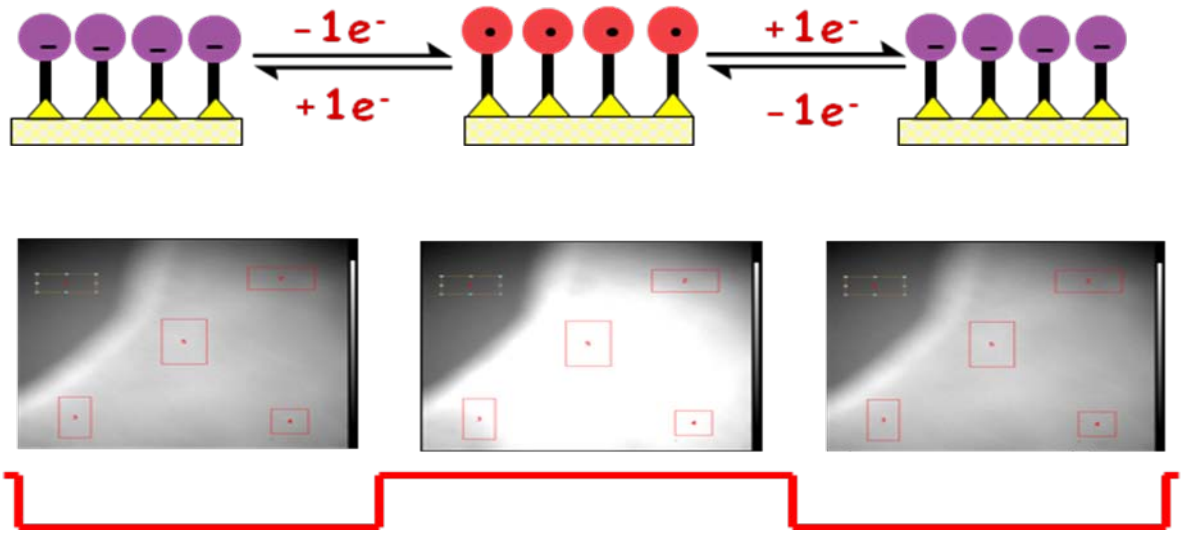

Figure S5 Fluorescence microscopy images of the SAM of **1** on ITO when consecutive write-erase cycles (+0.9V/-0.9V) were applied. The higher potential required in this experiment are probably due to a potential drop in the two-electrode configuration used.

Supplementary movie S1 corresponding to Figure S5

A)

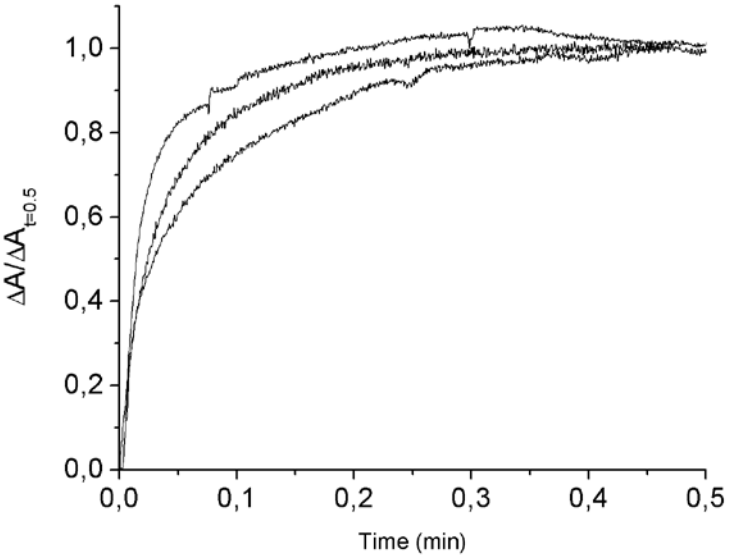

B)

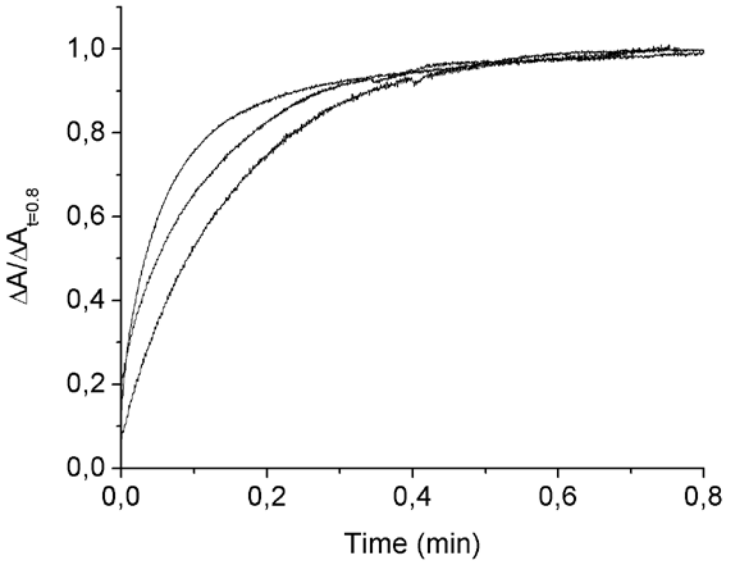

Figure S6. Voltage dependence of the UV-Vis absorbance of SAM of **1** along time when write/erase cycles were applied. *A)* Normalized absorbance at time 0.5 s ($\Delta A/\Delta A_{0.5}$), observed at 385 nm, using voltages of +0.3, +0.2, and +0.1 V, from top to bottom. B) Normalized absorbance at time 0.8 s ($\Delta A/\Delta A_{0.8}$), observed at 515 nm, at voltages of -0.3, -0.2, and -0.1 V, from top to bottom.

DOI: 10.1038/NCHEM.1013

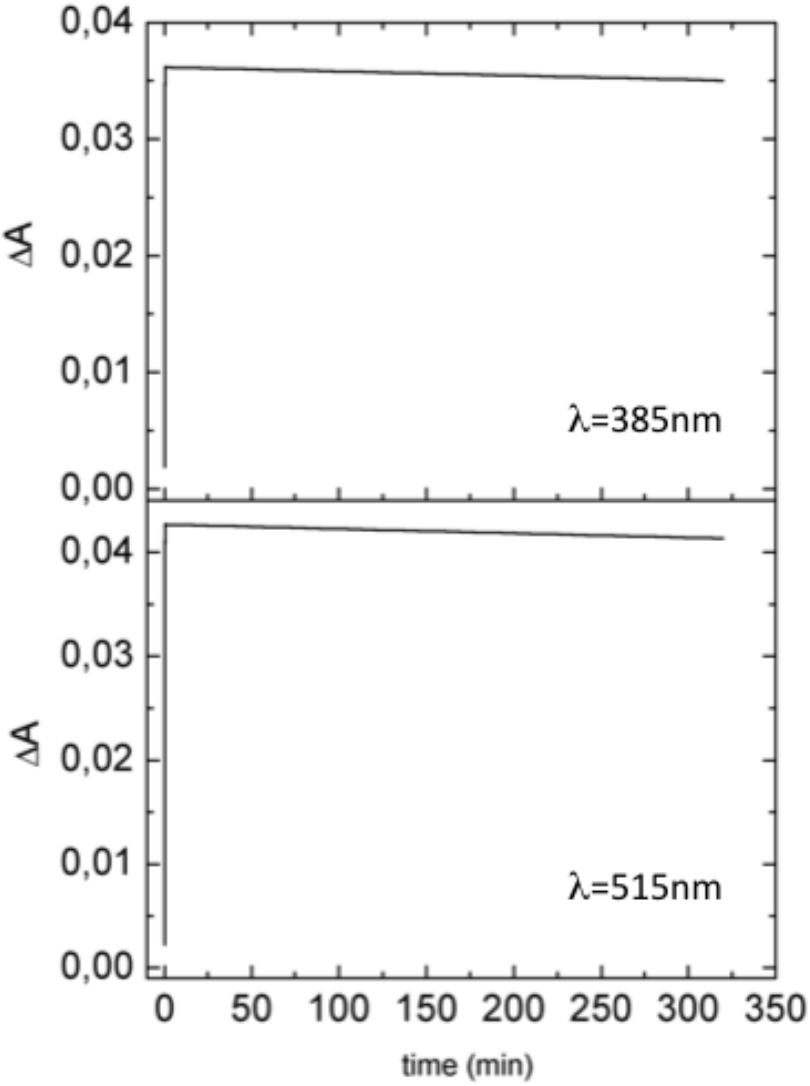

Figure S7. Absorbance changes of the SAMs of **1** in the radical **1**$^{\cdot}$ state (top), measured at 385 nm, and in the anion **1**$^{-}$ state (bottom), measured at 515 nm, along time when a voltage of +0.3 V or -0.3 V is applied to the substrate, respectively. As it can be seen, the absorbance intensity remains completely constant during many hours.

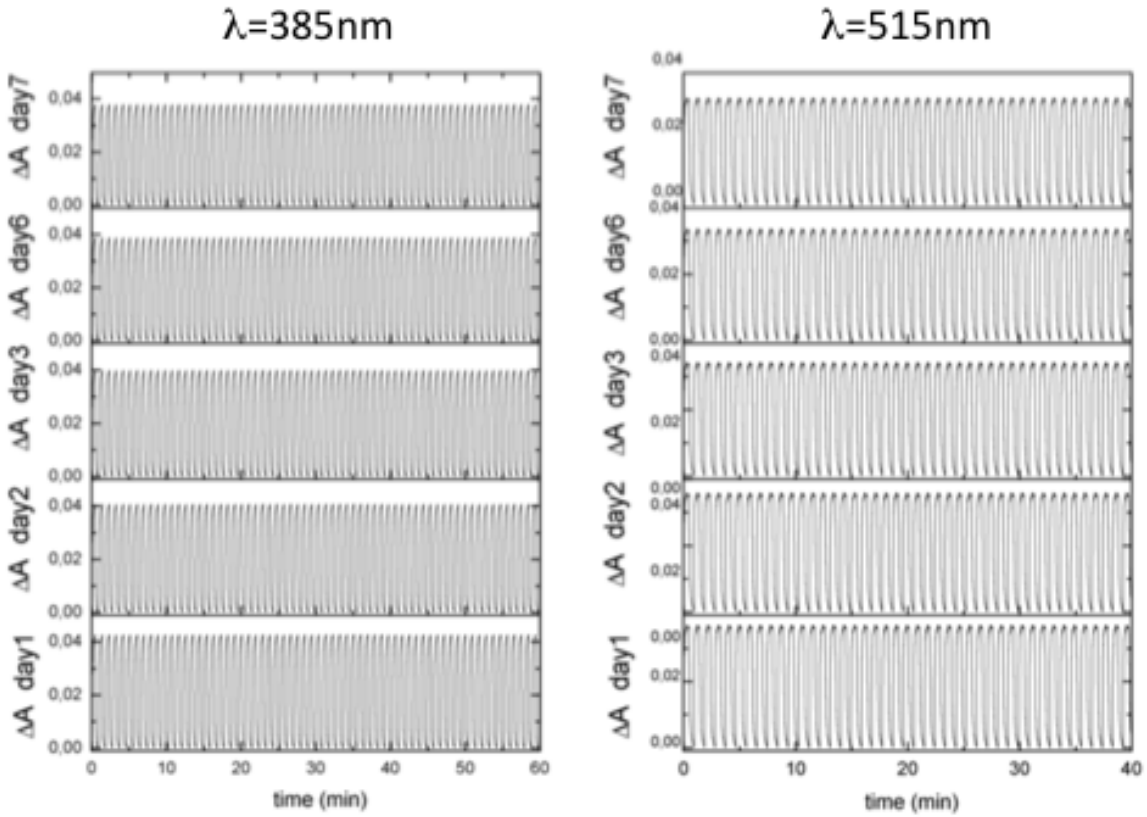

Figure S8. Study of the stability of the switch based on SAM of **1** during 7 days. Hundreds of write/erase (+0.3V/-0.3V) cycles were applied and the optical response at 385nm and 515 nm was monitored. The switch showed no hints of deterioration.

DOI: 10.1038/NCHEM.1013

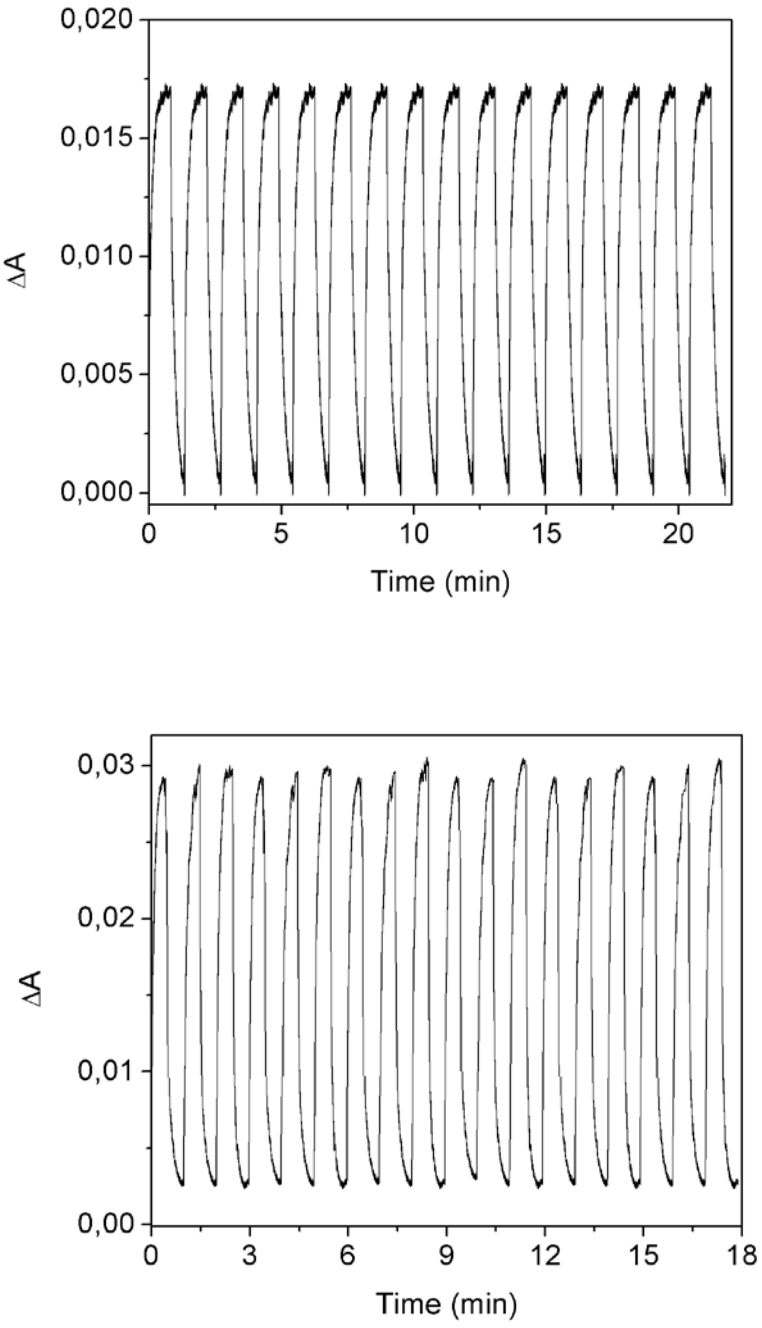

Figure S9. Switch response of the SAM of **1** upon application of cycles of +0.3/-0.3 V, measured 3 months after being prepared. *Top*, absorbance measured at 385 nm. *Bottom*, absorbance measured at 515 nm.

PATTERNED SURFACE

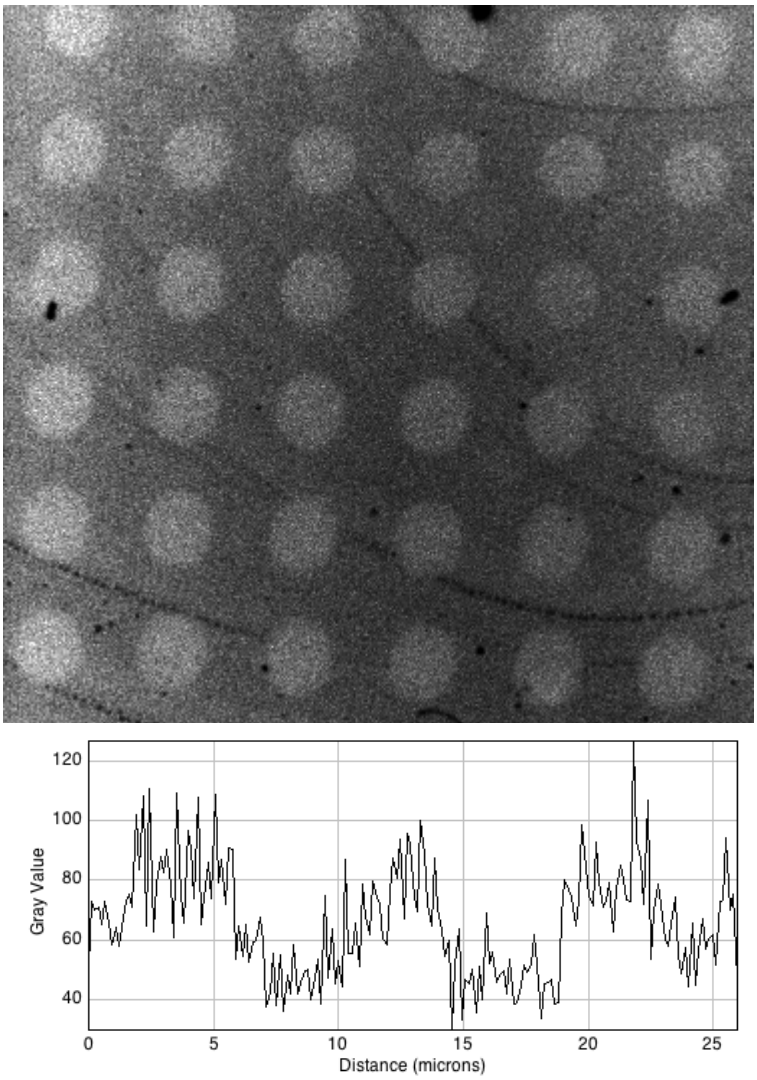

Figure S10. Fluorescence microscope image (λexcitation=340-370nm) of ITO patterned with **1.** The spots have a diameter of 5 μm.

DOI: 10.1038/NCHEM.1013

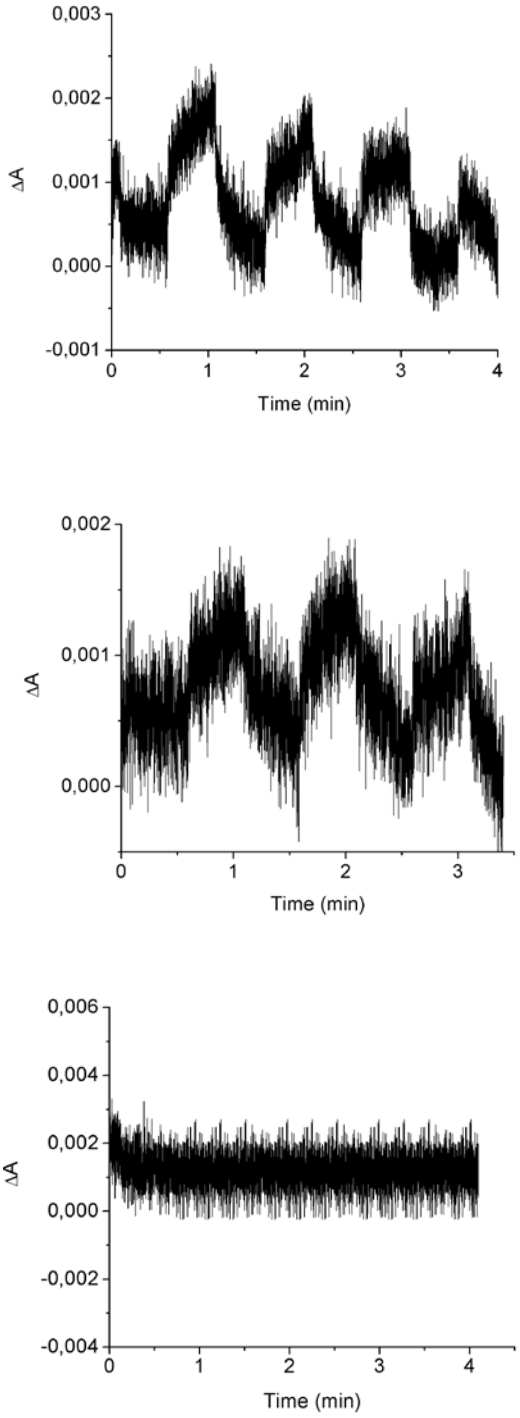

Figure S11. Switch responses of the SAM of **1** patterned as spots of 5 μm in diameter on an ITO surface, upon application of cycles of +0.3/-0.3 V. *Top*, changes monitored at 385nm. *Middle*, changes monitored at 515 nm. *Bottom*, blank ITO surface, upon application of cycles of +0.3/-0.3 V, monitored at 385nm as a control experiment. The large level of noise observed in all such measurements is due to: 1) The very small number of grafted molecules on the ITO surface produced by the short time (5 min) employed for the self-assembling of molecules during the μ-CP process, as compared with the longer time used in the non patterned surface (24 h). 2) The small size of patterned spots. 3) The fact that the surface for the non-patterned switches is a double face coated ITO glass.

LOCAL ADRESSABILITY

a)

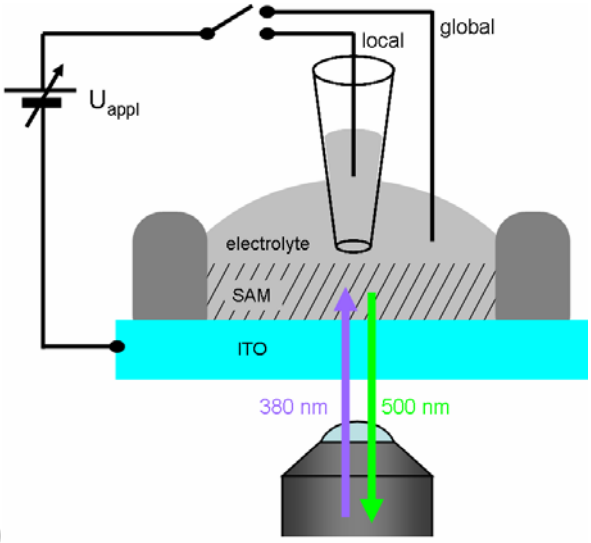

b)

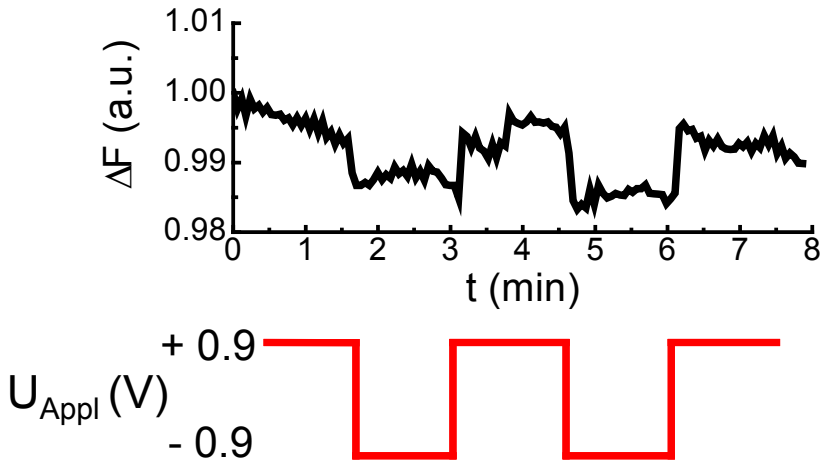

c)

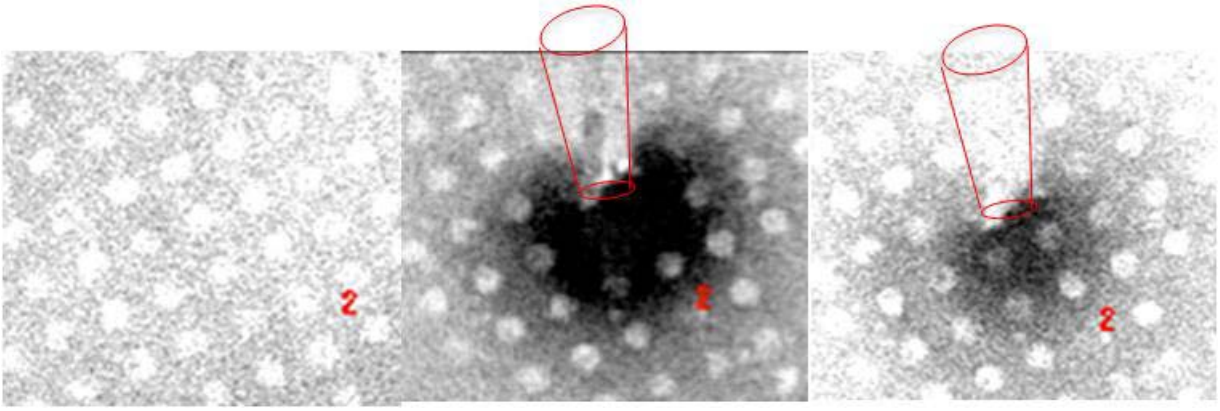

DOI: 10.1038/NCHEM.1013

Figure S12. Fluorescence switching and local addressability. a) Electrolyte chamber design for application of potentials to the entire PTM SAM (global) and through a microelectrode (local) during fluorescence imaging at 380 nm excitation and 500 nm emission. b) The fluorescence emission from PTM radical dots in patterned surface switches reversibly with the potential applied to the electrolyte ("global" electrode in (a)). c) Locally applying a potential through a microelectrode ("local" electrode in (a)) allows switching fluorescence reversibly (erase/write) from individual dots in a patterned PTM SAM.

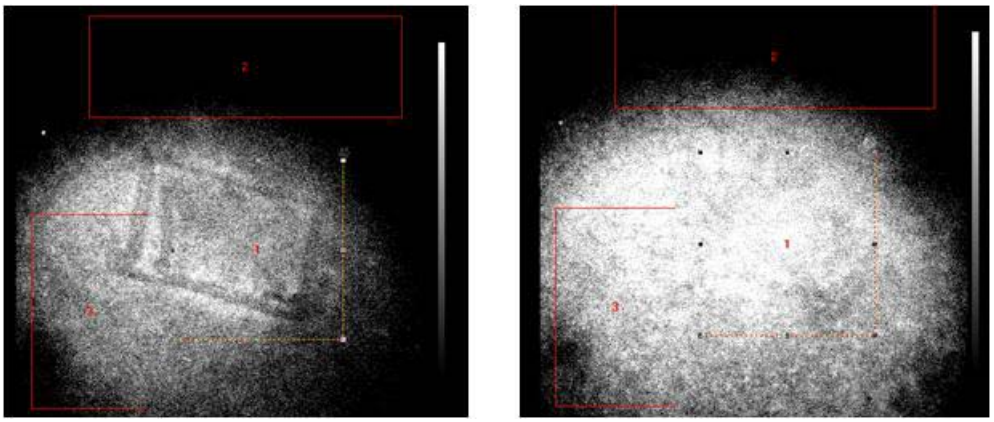

Figure S13. Local electrochemical writing and erasing . Fluorescence images of a PTM **1** SAM in which a rectangle and a line inside has been drawn by applying locally a negative potential through a microelectrode (left) and erasing of the rectangle and line by applying a positive potential to the ITO substrate (right)

Experimental setup for local oxidation/reduction of patterned PTM 1 SAMs and optical readout using fluorescence microscopy.

Electrolyte chambers were built on top of patterned PTM SAMS on ITO glass, using quick-dry silicone (Figure S11a) and imaged from below using fluorescence microscopy. Potentials were applied between the ITO and either a long, coiled silver wire immersed in the electrolyte (for oxidation/reduction of the entire film) or a microelectrode placed a few microns above the film (for local oxidation/reduction). Microelectrodes were fabricated from borosilicate capillary tubes using a P97 puller from Sutter Instruments in order to obtain a 1 μm diameter pipette. The pipette was filled with electrolyte. In an alternative approach, home-made polyethylene-insulated carbon fiber electrodes with a diameter of 12 μm were used for the experiments. Best results were obtained

with pulled glass microelectrodes (figure S11, S12). A mechanical/hydraulic micromanipulator (Narishige) was used to set the position of the microelectrode on the film. The potentials required for PTM **1** oxidation and reduction were relatively higher than in electrochemical recordings, probably due to a potential drop in the two-electrode configuration.